LANGMUIR

pubs.acs.org/Langmuir Article

Membrane Binding of Hydrophobic Ions: Application of New Kinetic Techniques

Alexander Baumgart, Do Trang Le, Charles G. Cranfield, Samara Bridge, Rocco Zerlotti, Ilaria Palchetti, Francesco Tadini-Buoninsegni, and Ronald J. Clarke*

Cite This: https://doi.org/10.1021/acs.langmuir.4c04779 Read Online

ACCESS | Metrics & More | Article Recommendations

ABSTRACT: Understanding membrane transport processes such as ion occlusion reactions of ion pumps and transporters and the ion gating of channels requires knowledge of lipid bilayer electrostatics. A simple example of the effect of membrane electrostatics on ion transport is the much higher permeability of the membrane to hydrophobic anions, such as tetraphenylborate (TPB^-), compared to hydrophobic cations, such as tetraphenylphosphonium (TPP^+) or tetraphenylarsonium (TPA^+). This has been attributed to the membrane dipole potential, of which a major contributor has been determined to be oriented water dipoles in the lipid headgroup region of the membrane. From the ratio of the TPB^- to TPP^+ or TPA^+ conductances, the magnitude and polarity of the dipole potential can be estimated. Using the voltage-sensitive dye RH421 in conjunction with the stopped-flow technique and solid-supported membrane electrophysiology here we show that the transport of these ions is not simply a diffusion through the membrane but rather occurs in jumps between discrete binding sites within the membrane. The hydrophobic anion TPB^- causes much greater RH421 spectral changes than TPA^+. This could be explained by a combination of a stronger interaction of TPB^- with RH421 and a deeper binding of TPB^- within the membrane compared to TPA^+. The experimental methods, used here for the first time to study the kinetics of ion transport across membranes, are potentially applicable to investigations of the membrane permeability of charged drug molecules, in particular anticancer agents.

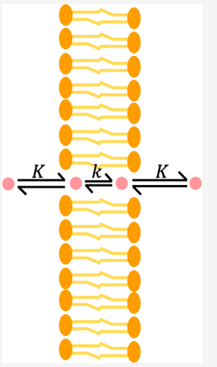

INTRODUCTION

Due to the anisotropic arrangement of the lipid molecules and their associated dipoles (including solvating water dipoles) in a lipid bilayer membrane, an electric field is present in the lipid headgroup region of the membrane. The electrical potential drop across the lipid headgroup region is termed the membrane dipole potential[1−6] (Figure 1).

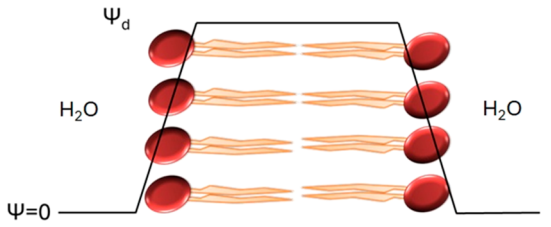

Figure 1. Schematic diagram showing the electrical potential, Ψ, profile across a membrane in the absence of any total transmembrane potential difference. As one enters the membrane and crosses the lipid headgroup region, Ψ becomes increasingly more positive, until one reaches the depth of the hydrocarbon tails. For simplicity, we assume that the electrical potential maintains a steady value across the hydrocarbon interior of the membrane. On the other side of the membrane, Ψ again drops to zero. The dipole potential, Ψ_d, which is positive in the membrane interior, is the electrical potential drop across the lipid headgroup region.

The first experimental indication of a membrane dipole potential and what its polarity might be came from electrical conductance measurements of bilayer lipid membranes in the presence of the hydrophobic or lipophilic ions, tetraphenylborate (TPB^-) and tetraphenylphosphonium (TPP^+) (Figure 2). Liberman and Topaly[7] found that adding either of these ions to the aqueous medium on each side of the membrane

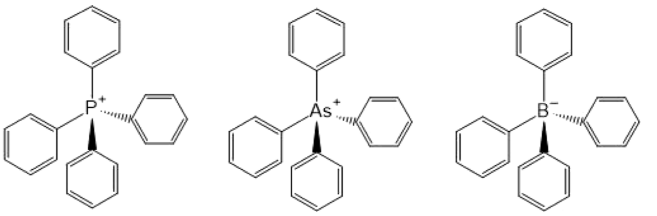

Figure 2. Structures of the hydrophobic ions, tetraphenylphosphonium (TPP^+), tetraphenylarsonium (TPA^+), and tetraphenylborate (TPB^-).

Received: November 25, 2024
Revised: March 11, 2025
Accepted: March 12, 2025

increased the membrane conductance. However, much higher concentrations of TPP^+ were required to produce the same increase in conductance caused by the addition of TPB^-. Based on the very similar chemical structures of the ions and assuming that the diffusion coefficients of both ions within the membrane are similar, Liberman and Topaly[7] attributed the different effects of the ions on membrane conductance to different partition coefficients of the differently charged ions between the membrane and aqueous phases, i.e., the negatively charged TPB^- partitions much more easily into the membrane than the positively charged TPP^+. They attributed this to the inner part of the membrane being positively charged, i.e., the membrane possesses a membrane dipole potential with a positive polarity; positive in the membrane interior relative to the membrane's interface with the adjacent aqueous solution.

Liberman and Topaly[7] did not estimate a value of the membrane dipole potential, but a number of other groups[8−12] subsequently used the relative conductances of membranes in the presence of TPB^- and TPP^+ or tetraphenylarsonium (TPA^+) to calculate a value for the dipole potential, ψ_d.

A more indirect method of quantifying the dipole potential involves using voltage-sensitive fluorescent dyes,[13−20] which, however, rely on independently determined values of ψ_d for calibration. Other methods of quantifying the dipole potential include the measurement of electrical surface potentials of lipid monolayers,[21−28] the intramembrane field compensation method[29−32] and cryo-electronmicroscopy.[33]

As pointed out by several authors,[9−11] calculation of a reliable value of the dipole potential from hydrophobic ion conductance measurements relies on a consideration of the different free energies of hydration of TPB^- and TPA^+. Theoretical calculations[34] indicate that TPB^- has a significantly stronger interaction with water than TPA^+ or TPP^+. The equation relating the conductances of the ions and their free energies of hydration, ΔG_{hyd}, is

$$\psi_d = \frac{RT}{2F}\ln\frac{g_{TPB^-}}{g_{TPA^+}} + \frac{\Delta G_{hyd}^{TPA+} - \Delta G_{hyd}^{TPB-}}{2F} \quad (1)$$

where R is the ideal gas constant, T is the absolute temperature, F is Faraday's constant and g is the specific conductance, i.e., the conductance per unit area of membrane per molar concentration of the hydrophobic ion (units: S cm^{-2} M^{-1}).

Measurements of membrane conductance in the presence of hydrophobic ions, however, provide little information on how the ions traverse the membrane or where within the membrane they bind. To provide more detailed information on the transport of these ions and to test the validity of predictions based on theoretical calculations we have used two complementary experimental approaches: stopped-flow kinetic measurements utilizing a voltage-sensitive fluorescent probe, RH421 (Figure 3), and a solid-supported membrane-based electrophysiological technique which relies on the principle of capacitive coupling. As far as we are aware, this is the first time that either of these techniques have been applied to study the membrane binding of hydrophobic ions, and the first time that the RH421 stopped-flow technique has been used to study the kinetics of interaction of any ion with membranes. Both methods are in principle applicable to the study of the kinetics of interaction of any charged species with membranes, including charged drug molecules. A further aim of the paper is, via kinetic measurements to determine the mechanism of transport of hydrophobic ions across lipid membranes.

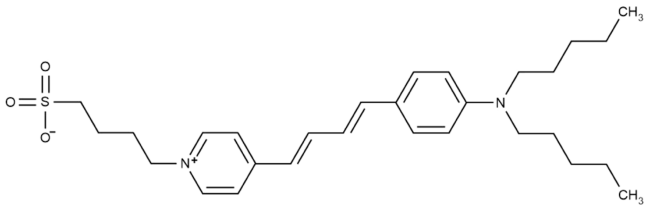

Figure 3. Structure of the voltage-sensitive styrylpyridinium dye RH421. The localized negative charge on the sulfonate group acts as a hydrophilic anchor, fixing this part of the molecule at the membrane/aqueous solution interface. The two alkyl chains at the other end of the molecule insert themselves into the hydrocarbon interior of the membrane, and the molecule's aromatic fluorophore is located within the lipid headgroup region of the membrane, coinciding with the site of the dipole potential drop. The fluorophore's positive charge is delocalized between the pyridinium and amino nitrogens. In the ground state the positive charge lies more on the pyridinium nitrogen, as shown in the figure. On electronic excitation, there is a large charge shift, with the positive charge moving toward the amino nitrogen. This makes the dye's UV/visible absorption spectrum and its fluorescence excitation spectrum very sensitive to the local electric field.[40]

Theoretical electrostatic energy calculations performed by Flewelling and Hubbell[35] indicate that TPP^+, and presumably also TPA^+, should bind a few Angstrom units closer to the membrane surface than TPB^-. A few Angstrom units may not seem like much, but the thickness of a lipid bilayer is typically 40−50 Angstrom units[36] and the dipole potential is thought to drop very rapidly across the lipid headgroup region, a distance of the order of only 10 Angstrom units.[1] Using nuclear magnetic resonance spectroscopy, Ellena et al.[37] found experimental evidence consistent with the theoretical predictions of Flewelling and Hubbell,[35] but the nuclear Overhauser effect method they employed was too insensitive to allow a difference in the binding depths of TPP^+ and TPB^- to be resolved. In contrast, based on an analysis of fluorescence titration results, Bühler et al.[38] suggested that TPP^+ should bind more toward the membrane interior than TPB^-. With the membrane dipole potential known to have a polarity which is positive on the inside of the membrane, it would seem counterintuitive that a positively charged ion should bind more deeply within the membrane. Nevertheless, a further aim of this paper is, therefore, to experimentally examine the binding of TPB^- and TPA^+ to model membrane systems to see whether Flewelling and Hubbell's theoretical predictions[35] are consistent with our experimental data or whether they support the conclusion of Bühler et al.[38]

It is worth noting that TPP^+ and TPA^+ are finding application as linkers to anticancer drugs[39] as a means of increasing uptake into cancer cells due to their hydrophobic nature and targeting mitochondria due to their positive charge and the high negative membrane potential of the inner mitochondrial membrane. Therefore, apart from their fundamental scientific value, the methods developed here and the results obtained are potentially of relevance to research in the field of cancer chemotherapy.

EXPERIMENTAL SECTION

Materials. *N*-(4-sulphobutyl)-4-(4-(p-(dipentylamino)phenyl)-butadienyl)-pyridinium inner salt (RH421) was synthesized by Vanessa V. Agon (University of Sydney) according to literature

https://doi.org/10.1021/acs.langmuir.4c04779
Langmuir XXXX, XXX, XXX−XXX

procedures.[41,42] Its purity as the E, E (all trans) isomeric form was verified as described previously.[43] 1,2-dimyristoylphosphatidylcholine (DMPC) and diphytanoylphosphatidylcholine (DPhPC) were purchased from Avanti Polar Lipids (Alabaster, AL, USA) and were used as received. The origins and purities of the other reagents used were: 1-octadecanethiol (98%, Sigma-Aldrich, Macquarie Park, Australia), chloroform (≥99.5%, Ajax Finechem, Scoresby, Australia), ethanol (≥99.9%, Merck, Bayswater, Australia), ethylenediamine tetraacetic acid (EDTA) (approximately 99%, Sigma-Aldrich), hydrochloric acid (0.1 N Titrisol solution, Merck), sodium chloride (≥99.5%, Merck), *n*-decane (≥99.5%, Sigma-Aldrich), tetraphenylarsonium chloride (97%, Fluka, Buchs, Switzerland), sodium tetraphenylborate (≥99.5%, Merck), and tris(hydroxymethyl)-aminomethane (Tris) (99%, Alfa Aesar, Heysham, UK). Purified water (18.2 MΩ) was obtained from a Millipore Direct-Q system.

Fluorescence Titrations. All fluorescence spectra and fluorescence titrations were performed using an RF-6000 spectrofluorophotometer (Shimadzu, Kyoto, Japan) using 1 cm path length quartz semimicrocuvettes. All fluorescence excitation spectra were recorded at an emission wavelength, λ_{em}, of 670 nm (bandwidth 5 nm) with an RG645 cutoff filter (Schott, Mainz, Germany) in front of the photomultiplier. For ratiometric measurements, the fluorescence ratio, *R*, was calculated as the ratio of the fluorescence emission intensity at an excitation wavelength of 440 nm divided by the fluorescence emission intensity at an excitation wavelength of 540 nm, following a method previously developed for the voltage-sensitive dye RH421.[44] On excitation RH421 undergoes a large charge shift, resulting in the positive charge, which was predominantly localized on the pyridinium nitrogen in the ground state, moving toward the amino nitrogen[45] (Figure 3). The large charge shift makes the dye's UV/visible absorbance and fluorescence spectra very sensitive to the polarity of its surroundings.[46] Via time-resolved fluorescence lifetime and anisotropy measurements it has been found that on binding of TPB^- to a membrane containing RH421, the dye undergoes a reorientation relative to the membrane surface.[47] Because the polarity of a membrane changes rapidly across the lipid headgroup region, where the dye is located, its reorientation causes a significant change in its local polarity, leading to spectral changes. This is termed a reorientational/solvatochromic mechanism. Some portion of RH421's fluorescence response to a change in electric field strength of its surroundings is likely also due to a pure electrochromic mechanism, which is not based on any movement of the dye molecule, but rather a change in energy required to bring about the electronic redistribution which occurs on transition to the excited state.

UV/Visible Absorbance Measurements. All UV/visible absorbance spectra were performed using a double-beam UV-2600i spectrophotometer (Shimadzu, Kyoto, Japan) using 1 cm path length quartz semimicrocuvettes. All spectra were recorded using a bandwidth of 5 nm. To accurately detect small absorbance changes and small wavelength shifts, 3.3 μL of a concentrated sodium tetraphenylborate stock solution of 15 mM in ethanol was added directly to a cuvette containing RH421 in ethanol, and the RH421 absorbance spectrum was corrected for dilution.

Stopped-Flow Spectrofluorimetry. Stopped-flow fluorescence experiments were carried out using an SF-61DX2 stopped-flow spectrophotometer (TgK Scientific, Bradford-on-Avon, UK). The solution in the observation chamber was excited by the 577 nm mercury line of a 75 W mercury−xenon arc lamp (Hamamatsu Photonics, Hamamatsu City, Japan) and the fluorescence was detected at right angles to the incident light using an R928 multialkali side-on photomultiplier (Hamamatsu). Fluorescence was collected at wavelengths ≥665 nm by using an RG665 glass cutoff filter (Schott, Mainz, Germany) in front of the photomultiplier. To improve the signal-to-noise ratio of the measured experimental traces, between 4 and 9 traces were averaged. The electrical time constant of the fluorescence detection system was set to 10 ms. As in previous studies using the voltage-sensitive fluorescent dye RH421,[48] interference from slow photochemical reaction of the dye was avoided by inserting an NG9 neutral density filter (Schott) in the light beam in front of the monochromator. Observed rate constants, k_{obs}, were derived from the observed kinetic traces by fitting a sum of exponential functions to the observed data using software supplied with the stopped-flow spectrophotometer.

The concentration of RH421 added to the DMPC vesicle suspension was 300 nM, i.e., 150 nM after mixing, because the instrument mixes equal volumes of the DMPC vesicle suspension and the TPB^- solution. Control experiments at lower RH421 concentrations of 75 and 37.5 nM after mixing yielded no significantly different values of the k_{obs} values. Therefore, it can be concluded that 150 nM of RH421 is not at a level which would have any effect on the kinetics of TPB^- interaction with the vesicles.

Lipid Vesicle Preparation. All lipid vesicles used in this study were prepared from DMPC via a modification of the ethanol injection method of Batzri and Korn.[49] Details of the method have been described previously.[50] The method involves injecting an ethanolic solution of lipid into buffer solution (30 mM Tris, 150 mM NaCl, 1 mM EDTA, adjusted to pH 7.2 with HCl) slowly with constant stirring and subsequently removing the ethanol by dialysis at 30 °C, i.e., above DMPC's main phase transition temperature of 23 °C. The method produces large unilamellar vesicles.

Solid-Supported Membrane-Based Electrophysiology. All solid-supported membrane-based electrophysiological measurements were performed using a surface electrogenic event reader ($SURFE^2R$) from Nanion Technologies (Munich, Germany). The $SURFE^2R$ sensors consist of a gold electrode to which a monolayer of octadecanethiol is covalently attached. A monolayer of lipid, in our case DPhPC, is then added on top of the octadecanethiol layer, forming a bilayer compound membrane. The detection of ion binding by the method relies on the principle that the compound membrane acts as a capacitor. However, in contrast to a typical electrical capacitor, where electrons bind to or are removed from the capacitor's plates until the capacitor is fully charged, ions bind from a flow circuit to the membrane surface. Nevertheless, just like in any capacitor, the charge that binds to one capacitor plate must be compensated by a counter movement of charge on the other plate, i.e., the gold electrode. Thus, if anions bind to the membrane, electrons must flow through the external circuit away from the gold electrode. Conversely, if cations bind to the membrane, electrons must flow through the external circuit toward the gold surface. In both cases a current is produced in the external circuit which one can measure.[51−53]

When ions bind to the membrane, this produces a capacitive current, $I(t)$, which first rises and then decays as the ion binding reaction comes into equilibrium. Once the system has reached equilibrium and the capacitive current has decayed, there remains a small stationary current, which can be considered as a baseline current and must be subtracted from the signal prior to any further analysis. The time course of the current signals obtained using the $SURFE^2R$ cannot be directly compared to the results obtained by the stopped-flow spectrofluorimetry, because current is the rate of movement of charge, whereas the stopped-flow signals are proportional to the amount of charge bound via its effect on the RH421 fluorescence. Therefore, the $SURFE^2R$ signals must first be integrated as a function of time to obtain $q(t)$, the charge bound at any time point. After this integration the $q(t)$ signals can then be fitted to sums of exponential time functions, just like the stopped-flow data, to obtain observed rate constants. The value of $q(t)$ at $t = \infty$, i.e., once the ion binding reaction has come into equilibrium and the capacitive current has decayed, yields the total charge, *Q*, that has bound to the membrane.

The experiments were carried out by flowing an activating solution containing either TPB^- or TPA^+ in buffer (30 mM Tris, 150 mM NaCl, 1 mM EDTA, pH 7.2) across the sensor membrane for 3 − 4 s, followed by a wash with nonactivating solution, i.e., buffer without TPB^- or TPA^+. The flow time was adjusted according to the kinetics of the reaction, i.e., for fast reactions where the capacitive current had already decayed to zero by 3 s, the flow time was reduced to this value. All measurements were carried out using a gain of 10^8 V/A. Further technical details of the $SURFE^2R$ instrument can be found in Tadini-Buoninsegni and Fendler,[54] Bazzone, Barthmes and Fendler,[55] and Bazzone and Barthmes.[56]

https://doi.org/10.1021/acs.langmuir.4c04779
Langmuir XXXX, XXX, XXX−XXX

RESULTS AND DISCUSSION

RH421 Fluorescence Titrations. The addition of TPA^+ to DMPC vesicles labeled with the voltage-sensitive fluorescent dye RH421 causes a very small blue shift in the dye's fluorescence excitation spectrum (Figure 4). This can be compared with previous results from our group,[46] showing that TPB^- causes a very significant red shift of the UV/visible absorbance spectrum of RH421, also when bound to DMPC vesicles (Figure 5). The directions of the shifts are consistent with TPA^+ increasing and TPB^- decreasing the inside-positive dipole potential. However, it is important to note that the magnitudes of the shifts are very different. If the two ions were binding within the membrane at the same location and there was no direct interaction between either of the ions and RH421, then at similar levels of the two ions within the membrane one would logically expect the magnitudes of the shifts in the RH421 spectra to be similar, because the local dielectric constant at the site of ion binding would be the same for both hydrophobic ions. This is obviously not the case. The spectral changes caused by TPB^- are much greater than those caused by TPA^+. This is qualitatively consistent with results from Bühler et al.,[38] who found that TPB^- caused much greater fluorescence changes than TPP^+. In terms of the magnitude of the changes, it is also consistent with results found for a series of other anions (Br^-, NO_3^-, I^-, SCN^- and ClO_4^-) and cations (Sr^{2+}, Ba^{2+}, Ca^{2+}, Mg^{2+}, La^{3+}).[57] The spectral changes caused by the anions were consistently much greater than those produced by the cations, even though the cations have larger charges. Clarke and Lüpfert,[57] attributed this to the anions binding more deeply within the membrane than the cations where the dielectric constant would be lower, thus producing a much larger change in the local electric field strength and hence a larger effect on the dye's fluorescence excitation spectrum. The local dielectric constant of lipid membranes is known to decrease rapidly as one proceeds across the lipid headgroup region into the membrane interior,[35] from a dielectric constant of 80 in the neighboring aqueous solution to a value of approximately 2 in the interior. A small variation in the depth that an ion binds within the membrane could, thus, cause a very significant change in the RH421 spectral changes that the ion produces.

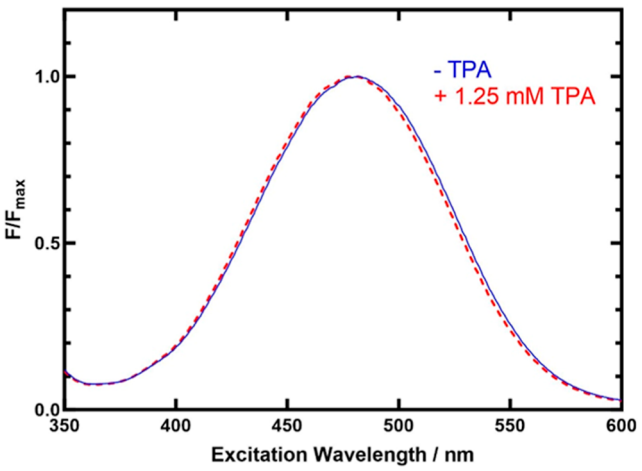

Figure 4. Fluorescence excitation spectra of RH421 (3.7 μM) in the presence of DMPC vesicles (200 μM lipid) before and after the addition of 1.25 mM of TPA^+. Because the TPA^+ was added from a 0.1 M stock solution in ethanol, the same volume of ethanol (11 μL) was added to the cuvette containing DMPC vesicles and RH421 alone to avoid the possibility of any spectral shifts arising from the ethanol addition. λ_{em} = 670 nm (+RG645 cutoff filter), excitation and emission bandwidths = 5 nm, T = 30 °C, pH 7.2.

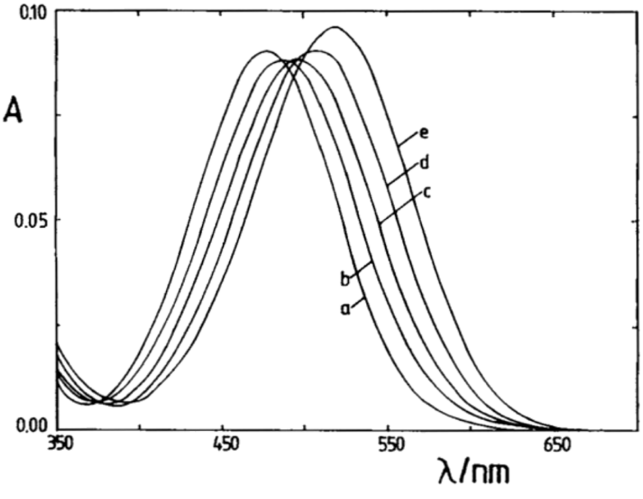

Figure 5. Absorbance spectra of RH421 (3.7 μM) in the presence of DMPC vesicles (200 μM lipid) as a function of the TPB^- concentration: (a) 0, (b) 5, (c) 10, (d) 20, and (e) 50 μM. T = 30 °C, pH 7.2 (reproduced from Clarke et al., 1995;[46] this article was published in the Biophysical Journal, Volume 68, Authors: RJ Clarke, A Zouni and JF Holzwarth, Title: Voltage sensitivity of the fluorescent probe RH421 in a model membrane system, pages 1406–1415. Copyright Elsevier 1995).

To investigate the possibility that the much greater RH421 spectral shifts caused by TPB^- in comparison to TPA^+ could be due to a direct interaction between TPB^- and the dye, absorbance spectra of RH421 in the presence and absence of TPB^- in ethanolic solution were recorded. Ethanol was chosen as the solvent because both RH421 and sodium tetraphenylborate have much higher solubilities in ethanol compared to water. In ethanolic solution TPB^-, at the highest concentration used for the membrane experiments of 50 μM, was found to have a small effect on the UV/visible absorbance spectrum of RH421 (Figure 6). On addition of TPB^-, a blue shift of the absorbance maximum of 1 nm occurred, from 517 nm in the absence of TPB^- to 516 nm in the presence of 50 μM of TPB^-. There was also a decrease in absorbance of 2.48% at 517 nm. This is in contrast to the effects of TPB^- in the presence of lipid vesicles, where TPB^- caused a red shift of approximately

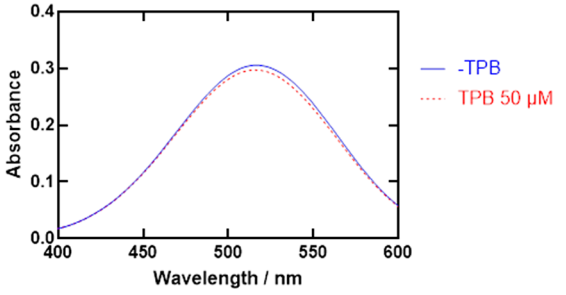

Figure 6. Absorbance spectra of RH421 (3.7 μM) in ethanolic solution before (blue) and after (red, dashed) the addition of 50 μM of TPB^- directly to the cuvette. The spectral bandwidth was 5 nM. The spectrum after TPB^- addition has been corrected for dilution.

https://doi.org/10.1021/acs.langmuir.4c04779
Langmuir XXXX, XXX, XXX−XXX

40 nm (from 480 nm without TPB^- to 520 nm with TPB^-) and an increase in absorbance of 6.8% (Figure 5).

The effects of TPB^- in the membrane are, thus, much greater than the effects in ethanolic solution and in the opposite directions in terms of both the wavelength and absorbance changes. The fact that the addition of TPB^- causes any change in the absorbance spectrum of RH421 at all indicates that a direct interaction between them can occur. The opposite directions of the RH421 wavelength and absorbance shifts after adding TPB^- is consistent with the RH421-TPB^- complex having an absorbance spectrum which is intermediate between RH421 bound to DMPC vesicles and RH421 in ethanol. The much greater spectral changes that occur in vesicles could easily be explained by a concentration of both RH421 and TPB^- in the membrane so that they are on average in much closer proximity to one another than when they are free to diffuse in an ethanolic solution. Therefore, the much larger spectral changes caused by TPB^- in membranes in comparison to TPA^+ could, in part, be explained by a stronger electrostatic interaction between RH421 and TPB^- than between RH421 and TPA^+. Another contributing factor, however, could be a difference in membrane binding depth of the two hydrophobic ions. If TPB^- binds more deeply within the membrane than TPA^+, in a region of lower polarity (lower dielectric constant) each TPB^- ion would produce a stronger electric field strength than each TPA^+ ion, thus causing a greater perturbation of RH421's conjugated π-electron system and greater spectral changes.

A significant difference between the results found here for TPA^+ and those found previously[57] for the divalent cations Sr^{2+}, Ba^{2+}, Ca^{2+}, Mg^{2+}, La^{3+} is that the signs of the spectral changes are opposite, i.e., TPA^+ causes a blue shift of the RH421 fluorescence excitation spectrum, whereas Sr^{2+}, Ba^{2+}, Ca^{2+}, Mg^{2+} and La^{3+} cause a red shift. This could be rationalized by the difference in the hydrophobicity of the ions. Whereas TPA^+ is a hydrophobic cation, Sr^{2+}, Ba^{2+}, Ca^{2+}, Mg^{2+} and La^{3+} are all hydrophilic. This difference in hydrophobicity is likely to influence the depth of binding of the ions within the membrane. The RH421 red shift caused by the hydrophilic cations is consistent with a decrease in the membrane dipole potential, which can be explained[57] by the ions binding at the membrane surface, most likely interacting with the negatively charged phosphate group of the lipid headgroup. The fact that TPA^+ causes a blue shift, would then imply that this ion binds further within the membrane than the hydrophilic cations and, therefore, is probably not interacting with the lipid's phosphate group.

To determine a dissociation constant for the interaction of TPA^+ with the membrane, a titration was performed over a range of TPA^+ concentrations. TPA^+ was added from a series of ethanolic stock solutions so that the amount of added ethanol was always constant and any possible spectral changes from ethanol addition could be avoided. Because the spectral changes are so small (Figure 4), the shift in the excitation spectrum caused by TPA^+ was quantified by a sensitive ratiometric method. The fluorescence ratio, R, was defined as the fluorescence intensity at an excitation wavelength of 440 nm divided by the intensity at an excitation wavelength of 540 nm. This is the same method that we have developed in previous studies.[15,44] The concentration dependence of R is shown in Figure 7. The data could be fitted to a hyperbolic binding curve described by eq 2

$$R = (R_{max} - R_{min})\frac{[TPA]}{(K_d + [TPA])} + R_{min} \quad (2)$$

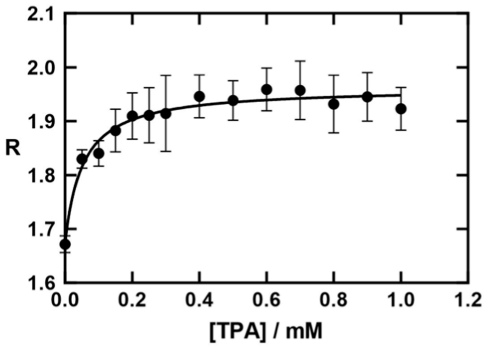

Figure 7. TPA^+ concentration dependence of the RH421 fluorescence ratio, R ($=F_{440}/F_{540}$). The concentration of RH421 was 3.7 μM and the DMPC concentration was 200 μM. λ_{em} = 670 nm (+RG645 cutoff filter), excitation and emission bandwidths = 5 nm, T = 30 °C, pH 7.2. The solid line represents a nonlinear least-squares fit of a hyperbolic binding curve to the data, as described by eq 2. The fitted parameters obtained were K_d = 52 (±13) μM, R_{min} = 1.67 (±0.02), and R_{max} = 1.96 (±0.01).

An alternative method of fitting the data would be to treat association of hydrophobic ions to the membrane as a partition between aqueous and membrane phases. Binding and partition models are, however, mathematically equivalent. There is a simple mathematical relationship between the dissociation constant, K, and the partition coefficient, γ.[58] In a binding model saturation occurs when all binding sites on the membrane are occupied, whereas in a partition model saturation occurs when the solubility limit of the substrate within the membrane phase is reached. However, we prefer to use a binding model, because the membrane is definitely not a homogeneous phase. As shown in Figure 1, the lipid molecules composing the membrane are arranged anisotropically, so that any ion associating with the membrane would experience a variation in its local chemical environment as it moved through the membrane, e.g. a variation in dielectric constant, as explained earlier. For this reason, it is to be expected that ions associating with a membrane would have energetically preferred locations, which we refer to as their binding sites.

Fitting of the TPA^+ fluorescence titration data shown in Figure 7 to eq 2 yielded a K_d of 52 (±13) μM. In the case of TPB^-, because the fluorescence changes are much bigger than those of TPA^+, we quantified the effect of TPB^- on the RH421 fluorescence by measuring the relative fluorescence change after TPB^- addition at a wavelength on the red edge of the dye's fluorescence excitation spectrum (Figure 8). Because this is a relative change, there is no y-intercept for the graph and the hyperbolic equation describing the binding is even simpler than eq 2, with only two fitting parameters, rather than three. The relevant equation is

$$\frac{\Delta F}{F_0} = \left(\frac{\Delta F}{F_0}\right)_{max} \frac{[TPB]}{(K_d + [TPB])} \quad (3)$$

Fitting of the TPB^- fluorescence titration data shown in Figure 8 to eq 3 yielded a K_d of 22 (±2) μM.

Stopped-Flow Fluorimetry. Due to the very small change in RH421 fluorescence caused by the interaction of TPA^+ with

https://doi.org/10.1021/acs.langmuir.4c04779
Langmuir XXXX, XXX, XXX−XXX

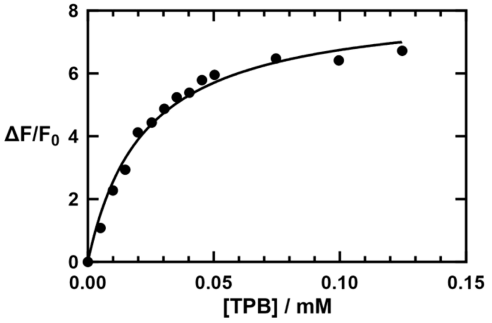

Figure 8. TPB^- concentration dependence of the RH421 relative fluorescence change, $\Delta F/F_0$, after addition of TPB^- to DMPC lipid vesicles (154 μM lipid) labeled with 3.7 μM RH421. λ_{ex} = 550 nm (+OG530 cutoff filter), λ_{em} = 660 nm (+RG645 cutoff filter), excitation and emission bandwidths = 3 nm, T = 30 °C, pH 7.2. $\Delta F/F_0$ represents the normalized fluorescence change, whereby F_0 is the fluorescence before the addition of TPB^-. The solid line represents a nonlinear least-squares fit of a hyperbolic binding curve to the data, as described by eq 3. The fitted parameters obtained were K_d = 22 (±2) μM, and $(\Delta F/F_0)_{max}$ = 8.3 (±2). Reproduced from ref 46. Copyright 1995 Elsevier.

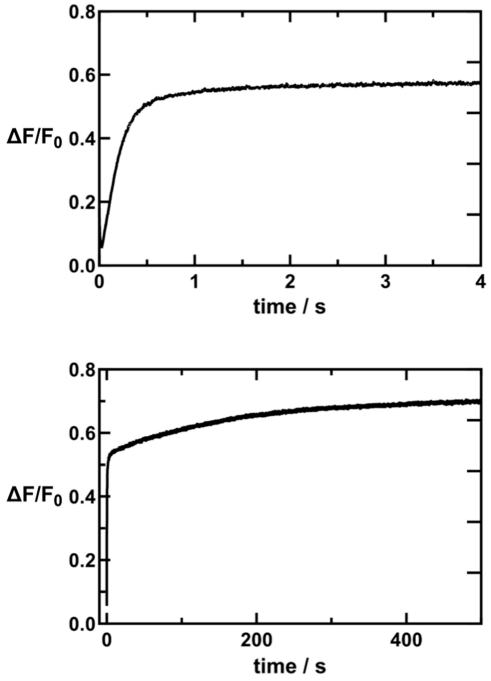

Figure 9. Stopped-flow fluorescence traces. TPB^- (final concentration 15 μM after mixing) was rapidly mixed with DMPC vesicles (200 μM of lipid after mixing) labeled with RH421 (150 nM after mixing). Both solutions were in a buffer containing 30 mM Tris, 150 mM NaCl, 1 mM EDTA, pH 7.2, and were thermostated to a temperature of 30 °C. The results show a biphasic behavior, with a rapid increase in fluorescence over approximately 1 s (upper trace), followed by a much slower increase over hundreds of seconds (lower trace). For these particular traces, the rapid phase (upper trace) could be fitted by a single exponential time function with an observed rate constant, k_{1obs}, of 5.94 (±0.02) s^{-1}. The slower phase (lower trace) could also be described by a single exponential time function, with an observed rate constant, k_{2obs}, of 4.33 (±0.01) × 10^{-3} s^{-1}.

DMPC vesicles (Figure 4), it was not possible to investigate the membrane binding of TPA^+ via the stopped-flow technique. Because the spectral changes caused by TPB^--binding were much greater, however (Figures 5 and 8), the kinetics of TPB^- interaction with DMPC vesicles could be investigated in detail. After rapid mixing of TPB^- with RH421-labeled DMPC vesicles (150 nM RH421 after mixing), two kinetic phases were observed. Both were characterized by an increase in RH421 fluorescence (Figure 9). This behavior is very reminiscent of previous studies of the kinetics of the interaction of potential-sensitive oxonol dyes with lipid vesicles, which also showed clear biphasic behavior.[58,59] In this case the results could be explained by a second-order binding of the dyes to the vesicle surface followed by a diffusion across the membrane from the outer to the inner lamella. It would seem likely that the same processes are occurring here in the case of TPB^-. To test this hypothesis, measurements were performed at both varying TPB^- and lipid concentrations.

The dependence of the observed rate constant, k_{1obs}, of the faster kinetic phase shows a linear dependence on the lipid concentration (Figure 10). This is analogous to the behavior previously observed for the oxonol dyes[58,59] and is typical for a second-order reaction, i.e., the binding of TPB^- to the vesicle surface. The slope of the graph yielded a second order rate constant, k_+, for the reaction of 2.7 (±0.08) × 10^5 M^{-1} s^{-1}.

The value of k_{1obs} of the faster phase also increased with the TPB^- concentration, but in this case the value saturated at a value of around 100 s^{-1} once the TPB^- concentration exceeded approximately 100 μM (see Figure 11). A possible explanation for saturation of the k_{1obs} value might be saturation of the TPB^- binding sites on the vesicle membrane surface. Because the data showed sigmoidal character, the phenomenological Hill eq (eq 4) was fitted to the data. This yielded values of k_{1max} = 102 (±4) s^{-1}, $K_{0.5}$ = 46 (±3) μM, and n_H = 2.9 (±0.4).

$$k = k_{max}\frac{1}{1 + (K_{0.5}/[TPB])^n H} \quad (4)$$

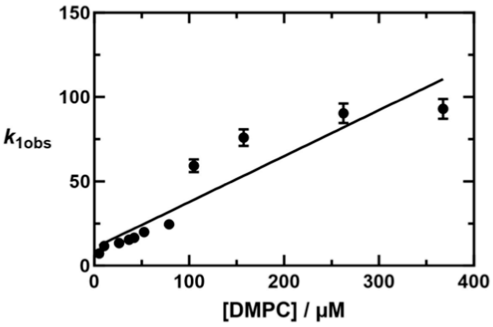

Figure 10. Dependence of the observed rate constant, k_{1obs}, of the faster kinetic phase observed on mixing of TPB^- (50 μM after mixing) with varying concentrations of DMPC lipid vesicles. The vesicles were noncovalently labeled with 150 nM (after mixing) of RH421. The buffer concentrations and temperature were as given in the caption of Figure 9. The slope of the graph corresponds to second order rate constant, k_+, of 2.7 (±0.08) × 10^5 M^{-1} s^{-1}.

The value of the observed rate constant for the slower kinetic phase, k_{2obs}, showed no obvious dependence on the TPB^- concentration.

In actual fact, the hydrophobic ions are not binding to an individual lipid molecule but to a vesicle, which could consist of many thousands of lipid molecules. Therefore, if one wished to determine whether or not binding of the hydrophobic ions

https://doi.org/10.1021/acs.langmuir.4c04779
Langmuir XXXX, XXX, XXX−XXX

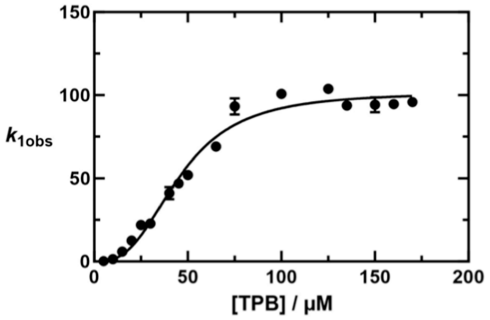

Figure 11. Dependence of the observed rate constant, k_{1obs}, of the faster kinetic phase observed on mixing of RH421-labeled lipid vesicles (200 μM lipid after mixing) with varying concentrations of TPB^-. Fitting of a Hill equation to the data yielded the following values: k_{1max} = 102 (±4) s^{-1}, $K_{0.5}$ = 46 (±3) μM, and n_H = 2.9 (±0.4). The buffer concentrations and temperature were as given in the caption of Figure 9.

to the vesicle was diffusion-controlled or not, one would need to obtain the slope of a plot of the observed rate constant for the fast phase versus the vesicle concentration. This point is further discussed and the necessary mathematical formalism developed in Clarke and Apell.[57]

A final point worth considering here is the RH421 concentration used for the stopped-flow measurements. Overall RH421 is a zwitterionic molecule (Figure 3), but the locations of its positive and negative charges relative to the membrane surface are very different. Whereas the negatively charged sulfonate group would be situated at the interface of the membrane with the aqueous solution, because of the dye's nonpolar hydrocarbon chains at the opposite end of the molecule, the dye's delocalized positive charge would be located further toward the membrane interior. The positive charge of the dye's styrylpyridinium chromophore could, in principle, affect the kinetics of TPB^- binding to the membrane. Indeed, micromolar concentrations of RH421 have been found to inhibit the kinetics of the membrane-bound ion pump, the Na^+, K^+-ATPase.[60] To avoid such inhibition, a submicromolar RH421 concentration of 150 nM was used for all of the stopped-flow measurements reported here.

Solid-Supported Membrane-Based Electrophysiology. In contrast to stopped-flow, the interaction of both TPB^- and TPA^+ with the supported membrane could be detected with the SURFE^{2}R instrument. The results obtained using the SURFE^{2}R cannot be quantitatively compared with those obtained via stopped-flow for a number of reasons. First, in the stopped-flow DMPC vesicles were used, whereas in the SURFE^{2}R measurements the lipid used was DPhPC. The reason DPhPC was preferred for the SURFE^{2}R was because its methyl side chains increase the strength of van der Waals interactions between neighboring lipid hydrocarbon chains, yielding a more stable membrane with no phase transition temperature between 0 and 100 °C. Another difference between the membrane used in the stopped-flow and SURFE^{2}R measurements was that the DMPC membrane used in stopped-flow contained DMPC in both lamellae, whereas the membrane used for the SURFE^{2}R was a hybrid membrane, with one lamella consisting of octadecanethiol covalently linked to the gold electrode surface and the other lamella consisting of DPhPC. A further difference was a technical one. In stopped-flow, rapid reactions can be resolved because the reagents are mixed within about a millisecond in a small reaction cell. In the SURFE^{2}R the time resolution is not as great because the entire solution must be exchanged from above the sensor surface in every measurement. Nevertheless,

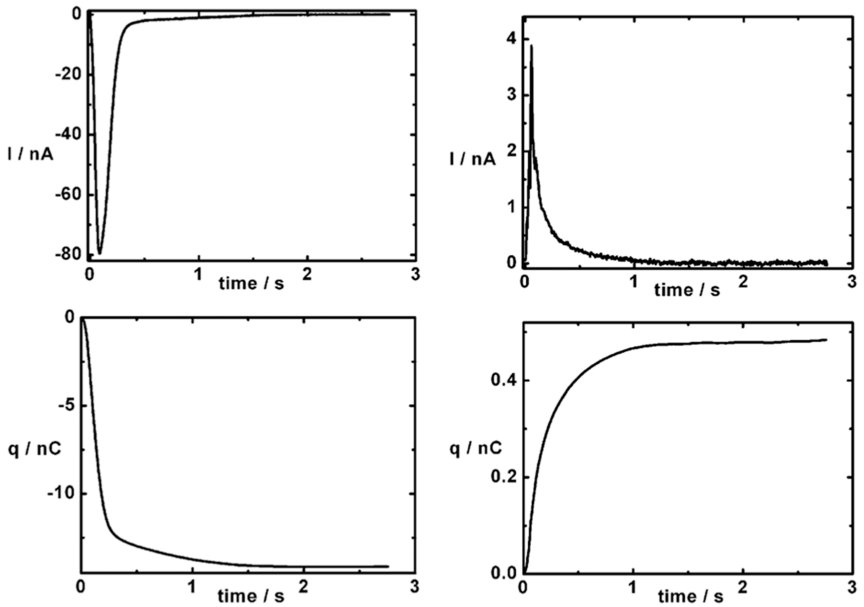

Figure 12. SURFE^{2}R results obtained on flowing solutions of TPB^- (100 μM), on the left, or TPA^+ (200 μM), on the right, over the membrane sensor surface. In both cases the hydrophobic ions were in a buffer solution containing 30 mM Tris, 150 mM NaCl, 1 mM EDTA, pH 7.2. The upper row shows the raw current transients obtained from the instrument. The lower row shows the corresponding charge build-up on the membrane sensor as a function of time, obtained by integrating the current transients. Both charge traces required at least two exponential time functions to reproduce the experimental curves. For TPB^- the two k_{obs} values were 9.45 (±0.05) s^{-1} (92% of the charge signal) and 1.09 (±0.05) s^{-1} (8% of the charge signal). For TPA^+ the two k_{obs} values were 15.58 (±0.08) s^{-1} (44% of the charge signal) and 3.098 (±0.004) s^{-1} (56% of the charge signal).

https://doi.org/10.1021/acs.langmuir.4c04779
Langmuir XXXX, XXX, XXX−XXX

despite these differences, qualitative comparisons can be made, and similarities in behavior can be identified.

The raw current traces obtained using the SURFE^{2}R are also not directly comparable with the stopped-flow fluorescence traces because, as described in the Materials section, the SURFE^{2}R traces first need to be integrated as a function of time to convert the $I(t)$ current curves into $q(t)$ charge curves. Once this is done (Figure 12), it can be seen that for TPB$^-$, the $q(t)$ curves are clearly biexponential, not single exponential. Although the time course is different to that obtained via stopped-flow, qualitatively it is the same. This indicates that the interaction of TPB$^-$ with the solid-supported membrane is a two-step process, presumably binding to the membrane surface followed by a slower diffusion further into the membrane.

In the case of TPA$^+$, it was not possible to resolve the kinetics of interaction with vesicles via stopped-flow because the changes in RH421 fluorescence were too small. This is, however, not the case with the SURFE^{2}R. Addition of TPA$^+$ to the membrane surface produced large positive currents, which could easily be detected (Figure 12). As in the case of TPB$^-$, the integrated charge $q(t)$ also shows a biexponential decay, indicative of a two-step binding process with the membrane. However, in the case of TPA$^+$, the kinetics of interaction are somewhat faster than those observed with TPB$^-$. To obtain information on the binding strength of the two ions to the SSM surface, the total integrated charges, Q, at the end of each transient were analyzed as a function of the hydrophobic ion concentration (Figure 13). A hyperbolic binding equation (eq 5), which has the same form as eq 3 that was used for the analysis of fluorescence titration data, was fitted to the experimental data.

$$Q = Q_{max}\frac{[\text{TPB or TPA}]}{(K_d + [\text{TPB or TPA}])} \quad (5)$$

This yielded K_d values of 180 (±60) μM for TPA$^+$ and 10 (±2) μM for TPB$^-$. As found via RH421 fluorescence measurements using DMPC vesicles, the K_d of TPA$^+$ is significantly higher than that of TPB$^-$, indicating a weaker binding of TPA$^+$ to the membrane than TPB$^-$. The magnitude of the charge bound at saturation is also much greater for TPB$^-$ (19.2 (±0.6) nC) than for TPA$^+$ (1.7 (±0.2) nC).

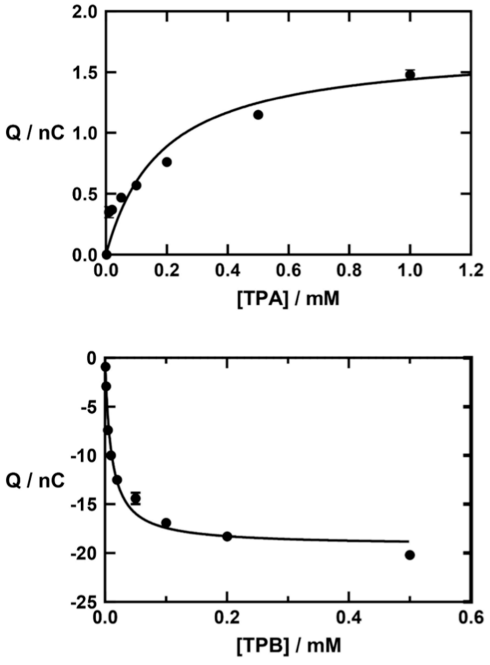

Figure 13. Dependence of the total integrated current, Q, obtained in SURFE^{2}R measurements on the concentrations of TPB$^-$ and TPA$^+$. Fitting of a hyperbolic binding equation to the data yielded the following values for TPA$^+$: K_d = 180 (±60) μM, and Q_{max} = 1.7 (±0.2) nC. The same fitting procedure for TPB$^-$ yielded the following values: K_d = 10 (±2) μM, and Q_{max} = −19.2 (±0.6) nC. The buffer composition was as given in the caption of Figure 12.

DISCUSSION

The membrane dipole potential is an electrical potential difference within cell membranes that is expected to have an important role in controlling or affecting the kinetics of conformational changes of membrane proteins, e.g., the ion occlusion reactions of ion pumps and the gating of ion channels.[61−63] The differences in membrane conductance caused by the addition of the hydrophobic anion, TPB$^-$, and the hydrophobic cations, TPP$^+$ and TPA$^+$, allow the magnitude and polarity of the dipole potential to be calculated. After correction for the ions' different hydration energies in the aqueous solution adjacent to the membrane, for a fully saturated phosphatidylcholine membrane the dipole potential has been estimated to be approximately +350 mV,[34] i.e., positive in the membrane interior. This produces enormous electric field strengths in the lipid headgroup region of the membrane of the order of 10^9 V m^{-1}, which is approximately 2 orders of magnitude greater than the electric field strengths produced by the transmembrane potential.[2] Transmembrane potentials are known to control the opening and closing of voltage-gated ion channels. It is, therefore, to be expected that changes in the dipole potential should have significant effects on the kinetics of electrogenic, i.e., charge-translocating steps of membrane proteins.[61−63]

Figure 1 is a simple schematic diagram showing the location of the dipole potential. For the discussion of the kinetics of hydrophobic ion interaction with a membrane let us take the example of TPB$^-$. The kinetics of interaction of TPB$^-$ with a membrane, M, can be described by the following mechanism:

$$TPB^- + M \overset{K}{\leftrightarrow} TPB^-M' \overset{k}{\rightarrow} TPB^-M''$$

Analogous mechanisms could, however, also be written for TPP$^+$ or TPA$^+$. TPB$^-$M′ represents here TPB$^-$ bound to the outer lamella of a membrane, whereas TPB$^-$M″ represents TPB$^-$ bound to the inner lamella of the membrane. The mechanism thus describes a fast binding of TPB$^-$ to the membrane followed by a slower transport step of TPB$^-$ moving across the membrane, with the first step being in a fast equilibrium on the time scale of the subsequent transport across the membrane. This is consistent with the observed experimental behaviors in the stopped-flow (Figure 9) and SURFE^{2}R experiments ($q(t)$ curves of Figure 12), where biphasic kinetics were observed in both cases.

The mechanism assumes that, like on the outer lamella, the dissociation of TPB$^-$ from the inner lamella into the adjacent aqueous solution is a rapid equilibrium step and is, therefore, not rate-determining for the overall transport of TPB$^-$ between the aqueous solutions on each side of the membrane. The rate-determining step is hence the jump of TPB$^-$ from the binding

https://doi.org/10.1021/acs.langmuir.4c04779
Langmuir XXXX, XXX, XXX−XXX

site on the outer lamella of the membrane to the binding site on the inner lamella, i.e.

$$\frac{d[\mathrm{TPB^-M''}]}{dt} = k[\mathrm{TPB^-M'}] \quad (6)$$

Because $\mathrm{TPB^-M'}$ is in equilibrium with $\mathrm{TPB^-}$ and M via the first reaction step $[\mathrm{TPB^-M'}]$ can be replaced in this differential rate equation by $K[\mathrm{TPB^-}][\mathrm{M}]$. This yields the equation

$$\frac{d[\mathrm{TPB^-M''}]}{dt} = kK[\mathrm{TPB^-}][\mathrm{M}] \quad (7)$$

The conductance of the membrane in the presence of $\mathrm{TPB^-}$ is, thus, determined by the product of the equilibrium constant for $\mathrm{TPB^-}$ binding to the membrane multiplied by the rate constant for $\mathrm{TPB^-}$ jumping across the membrane from the outer to the inner lamella, kK. An analogous conclusion has previously been reached by Pickar and Benz.[10] [M] in eq 7 requires some explanation. Because $\mathrm{TPB^-}$ is actually interacting with a binding site on the membrane, [M] would represent the concentration of free membrane binding sites, as previously defined for the interaction of a potential-sensitive dye with membrane vesicles.[58]

CONCLUSION

The results shown in Figures 4−9 using the voltage-sensitive fluorescent dye RH421 show that $\mathrm{TPB^-}$ produces much larger spectral changes than $\mathrm{TPA^+}$. Two factors could contribute to this. One is a stronger electrostatic interaction between $\mathrm{TPB^-}$ and RH421 than between $\mathrm{TPA^+}$ and RH421. The other contributing factor could be that $\mathrm{TPB^-}$ binds more deeply within the membrane than $\mathrm{TPA^+}$ and produces a stronger electric field strength due to a lower local dielectric constant. In the $\mathrm{SURFE^2R}$ measurements (Figures 12 and 13), $\mathrm{TPB^-}$ produces significantly larger capacitive currents than $\mathrm{TPA^+}$. The $\mathrm{SURFE^2R}$ measurements suggest that $\mathrm{TPB^-}$ binds more deeply within the membrane than $\mathrm{TPA^+}$. If $\mathrm{TPB^-}$ binds more deeply into the membrane interior than $\mathrm{TPA^+}$, one would expect it to experience a less polar membrane environment with a lower dielectric constant and, thus, produce greater changes in the local electric field and greater capacitive currents detected by the $\mathrm{SURFE^2R}$. These experimental results are consistent with the theoretical calculations performed by Flewelling and Hubbell,[35] which also predicted that hydrophobic cations would bind slightly closer to the membrane surface than hydrophobic anions.

Another important finding here is that the movement of hydrophobic ions across a membrane is a three-step process, i.e., binding of the ion to the outer leaflet of the membrane, jumping across the membrane interior to binding sites on the inner membrane leaflet and dissociation of the ion from the inner leaflet into the adjacent aqueous solution. The first two of these steps are most clearly shown by stopped-flow traces observed on mixing $\mathrm{TPB^-}$ with lipid vesicles (Figure 9). The $q(t)$ curves observed in the $\mathrm{SURFE^2R}$ measurements also show a biexponential decay (Figure 12), indicative of a two-step binding process with the membrane. It seems very likely that these two steps involve a fast binding of the ion to the membrane followed by a slower diffusion across it. If diffusion across the membrane were faster than binding, such that diffusion was always in equilibrium on the time scale of binding, then one would have expected a single exponential relaxation rather than two.

Very similar behavior has previously been observed on binding of negatively charged oxonol dyes with lipid vesicles.[58,59] In this case, however, the binding of the oxonol dyes to the membrane itself caused a fluorescence change. Therefore, it was not necessary to label the membrane with a voltage-sensitive dye, such as RH421, to follow the kinetics. The method developed here, whereby vesicles are first labeled with a voltage-sensitive styrylpyridinium dye is in principle applicable to studying the interaction of any small, charged molecule with membranes. Therefore, it would potentially allow the kinetics of cell uptake of charged drug molecules through the lipid membrane to be determined.

AUTHOR INFORMATION

Corresponding Author

Ronald J. Clarke − *School of Chemistry, University of Sydney, Camperdown, New South Wales 2006, Australia;* orcid.org/0000-0002-0950-8017; Email: Ronald.Clarke@sydney.edu.au

Authors

Alexander Baumgart − *School of Chemistry, University of Sydney, Camperdown, New South Wales 2006, Australia*

Do Trang Le − *School of Life Sciences, University of Technology Sydney, Ultimo, New South Wales 2007, Australia*

Charles G. Cranfield − *School of Life Sciences, University of Technology Sydney, Ultimo, New South Wales 2007, Australia;* orcid.org/0000-0003-3608-5440

Samara Bridge − *School of Life Sciences, University of Technology Sydney, Ultimo, New South Wales 2007, Australia*

Rocco Zerlotti − *Nanion Technologies, Munich D-80339, Germany*

Ilaria Palchetti − *Department of Chemistry "Ugo Schiff", University of Florence, Metropolitan 50019, Italy;* orcid.org/0000-0001-9366-0574

Francesco Tadini-Buoninsegni − *Department of Chemistry "Ugo Schiff", University of Florence, Metropolitan 50019, Italy;* orcid.org/0000-0001-5594-2554

Complete contact information is available at: https://pubs.acs.org/10.1021/acs.langmuir.4c04779

Notes

The authors declare no competing financial interest.

ACKNOWLEDGMENTS

R.J.C. acknowledges with gratitude financial assistance from the Australian Research Council (DP170101732) and the Faculty of Science, University of Sydney. The authors thank Isabella Felli for help with figure preparation, Zihan Zhou for helpful discussions and Toby Samuel for assistance with UV/visible absorbance measurements.

REFERENCES

(1) Brockman, H. Dipole potential of lipid membranes. *Chem. Phys. Lipids* **1994**, *73*, 57−79.

(2) Clarke, R. J. The dipole potential of phospholipid membranes and methods for its detection. *Adv. Colloid Interface Sci.* **2001**, *89*−*90*, 263−281.

(3) O'Shea, P. Intermolecular interactions with/within cell membranes and the trinity of membrane potentials: kinetics and imaging. *Biochem. Soc. Trans.* **2003**, *31*, 990−996.

https://doi.org/10.1021/acs.langmuir.4c04779
Langmuir XXXX, XXX, XXX−XXX

(4) Wang, L. Measurements and implications of the membrane dipole potential. *Annu. Rev. Biochem.* **2012**, *81*, 615−635.
(5) Ostroumova, O. S.; Efimova, S. S.; Malev, V. V. Modifiers of membrane dipole potentials as tools for investigating ion channel formation and functioning. *Int. Rev. Cell Mol. Biol.* **2015**, *315*, 245−297.
(6) Ermakov, Y. A. Electric fields at the lipid membrane interface. *Membranes* **2023**, *13*, 883.
(7) Liberman, Y. A.; Topaly, V. P. Permeability of bimolecular phospholipid membranes for fat-soluble ions. *Biofizika* **1969**, *14*, 452−461.
(8) Szabo, G. Dual mechanism for the action of cholesterol on membrane permeability. *Nature* **1974**, *252*, 47−49.
(9) Andersen, O. S.; Fuchs, M. Potential energy barriers to ion transport within lipid bilayers. Studies with tetraphenylborate. *Biophys. J.* **1975**, *15*, 795−830.
(10) Pickar, A. D.; Benz, R. Transport of oppositely charged lipophilic probe ions in lipid bilayer membranes having various structures. *J. Membr. Biol.* **1978**, *44*, 353−376.
(11) Gawrisch, K.; Ruston, D.; Zimmerberg, J.; Parsegian, V. A.; Rand, R. P.; Fuller, N. Membrane dipole potentials, hydration forces, and the ordering of water at membrane surfaces. *Biophys. J.* **1992**, *61*, 1213−1223.
(12) Peterson, U.; Mannock, D. A.; Lewis, R. N. A. H.; Pohl, P.; McElhaney, R. N.; Pohl, E. Origin of membrane dipole potential: Contribution of phospholipid fatty acid chains. *Chem. Phys. Lipids* **2002**, *117*, 19−27.
(13) Gross, E.; Bedlack, Jr. R. S.; Loew, L. M. Dual-wavelength ratiometric fluorescence measurement of the membrane dipole potential. *Biophys. J.* **1994**, *67*, 208−216.
(14) Bedlack, Jr. R. S.; Wei, M.; Fox, S. H.; Gross, E.; Loew, L. M. Distinct electric potentials in soma and neurite membranes. *Neuron* **1994**, *13*, 1187−1193.
(15) Clarke, R. J. Effect of lipid structure on the dipole potential of phosphatidylcholine bilayers. *Biochim. Biophys. Acta, Biomembr.* **1997**, *1327*, 269−278.
(16) Klymchenko, A. S.; Duportail, G.; Mély, Y.; Demchenko, A. P. Ultrasensitive two-color fluorescence probes for dipole potential in phospholipid membranes. *Proc. Natl. Acad. Sci. U.S.A.* **2003**, *100*, 11219.
(17) Starke-Peterkovic, T.; Turner, N.; Else, P. L.; Clarke, R. J. 2005. Electric field strength of membrane lipids from vertebrate species: Membrane lipid composition and Na^+,K^+-ATPase activity. *Am. J. Physiol.: Regul., Integr. Comp. Physiol.* **2005**, *288*, R663−R670.
(18) Warshaviak, D. T.; Muellner, M. J.; Chachisvilis, M. Effect of membrane tension on the electric field and dipole potential of lipid bilayer membrane. *Biochim. Biophys. Acta, Biomembr.* **2011**, *1808*, 2608−2617.
(19) Haldar, S.; Kanaparthi, R. K.; Samanta, A.; Chattopadhyay, A. Differential effect of cholesterol and its biosynthetic precursors on membrane dipole potential. *Biophys. J.* **2012**, *102*, 1561−1569.
(20) Kovács, T.; Batta, G.; Zákány, F.; Szöllősi, J.; Nagy, P. The dipole potential correlates with lipid raft markers in the plasma membrane of living cells. *J. Lipid Res.* **2017**, *58*, 1681−1691.
(21) Haydon, D. A.; Myers, V. B. Surface charge, surface dipoles and membrane conductance. *Biochim. Biophys. Acta* **1973**, *307*, 429−443.
(22) Hladky, S. B.; Haydon, D. A. Membrane conductance and surface potential. *Biochim. Biophys. Acta* **1973**, *318*, 464−468.
(23) Haydon, D. A.; Elliott, J. R. Surface potential changes in lipid monolayers and the 'cut-off' in anaesthetic effects of N-alkanols. *Biochim. Biophys. Acta, Biomembr.* **1986**, *863*, 337−340.
(24) Smaby, J. M.; Brockman, H. L. Surface dipole moments of lipids at the argon-water interface. Similarities among glycerol-ester-based lipids. *Biophys. J.* **1990**, *58*, 195−204.
(25) Moncelli, M. R.; Becucci, L.; Buoninsegni, F. T.; Guidelli, R. Surface dipole potential at the interface between water and self-assembled monolayers of phosphatidylserine and phosphatidic acid. *Biophys. J.* **1998**, *74*, 2388−2397.
(26) Maggio, B. Modulation of phospholipase A2 by electrostatic fields and dipole potential of glycosphingolipids in monolayers. *J. Lipid Res.* **1999**, *40*, 930−939.
(27) Luzardo, M.; del, C.; Amalfa, F.; Nuñez, A. M.; Diaz, S.; Biondi de Lopez, A. C.; Disalvo, E. A. Effect of trehalose and sucrose on the hydration and dipole potential of lipid bilayers. *Biophys. J.* **2000**, *78*, 2452−2458.
(28) Becucci, L.; Moncelli, M. R.; Herrero, R.; Guidelli, R. Dipole potentials of monolayers of phosphatidylcholine, phosphatidylserine, and phosphatidic acid on mercury. *Langmuir* **2000**, *16*, 7694−7700.
(29) Sokolov, V. S.; Kuzmin, V. G. Study of surface-potential difference in bilayer-membranes according to the 2nd harmonic response of capacitance current. *Biofizika* **1980**, *25*, 170−172.
(30) Sokolov, V. S.; Cherny, V. V.; Markin, V. S. Measurements by inner field compensation method of the potentials induced by phloretin and phloretin adsorption on BLM. *Biofizika* **1984**, *29*, 424−429.
(31) Malkov, D. Y.; Sokolov, V. S. Fluorescent styryl dyes of the RH series affect a potential drop on the membrane/solution boundary. *Biochim. Biophys. Acta, Biomembr.* **1996**, *1278*, 197−204.
(32) Ermakov, Y. A.; Averbakh, A. Z.; Yusipovich, A. I.; Sukharev, S. Dipole potentials indicate restructuring of the membrane interface by gadolinium and beryllium ions. *Biophys. J.* **2001**, *80*, 1851−1862.
(33) Wang, L.; Bose, P. S.; Sigworth, F. J. Using cryo-EM to measure the dipole potential of a lipid membrane. *Proc. Natl. Acad. Sci. U.S.A.* **2006**, *103*, 18528−18533.
(34) Schamberger, J.; Clarke, R. J. Hydrophobic ion hydration and the magnitude of the dipole potential. *Biophys. J.* **2002**, *82*, 3081−3088.
(35) Flewelling, R. F.; Hubbell, W. L. The membrane dipole potential in a total membrane potential model. Applications to hydrophobic ion interactions with membranes. *Biophys. J.* **1986**, *49*, 541−552.
(36) Regan, D.; Williams, J.; Borri, P.; Langbein, W. Lipid bilayer thickness measured by quantitative DIC reveals phase transitions and effects of substrate hydrophilicity. *Langmuir* **2019**, *35*, 13805−13814.
(37) Ellena, J. F.; Dominey, R. N.; Archer, S. J.; Xu, Z.-C.; Cafiso, D. S. Localization of hydrophobic ions in phospholipid bilayers using 1H Nuclear Overhauser Effect spectroscopy. *Biochemistry* **1987**, *26*, 4584−4592.
(38) Bühler, R.; Stürmer, W.; Apell, H. . −J.; Läuger, P. Charge translocation by the Na,K−pump: I. Kinetics of local field changes studied by time-resolved fluorescence measurements. *J. Membr. Biol.* **1991**, *121*, 141−161.
(39) Battogtokh, G.; Choi, Y. S.; Kang, D. S.; Park, S. J.; Shim, M. S.; Huh, K. M.; Cho, Y.-Y.; Lee, J. Y.; Lee, H. S.; Kang, H. C. Mitochondria-targeting drug conjugates for cytotoxic, anti-oxidizing and sensing purposes: current strategies and future perspectives. *Acta Pharm. Sin. B* **2018**, *8*, 862−880.
(40) Loew, L. M.; Bonneville, G. W.; Surow, J. Charge shift optical probes of membrane potential. Theory. *Biochemistry* **1978**, *17*, 4065−4071.
(41) Grinvald, A.; Hildesheim, R.; Farber, I. C.; Anglister, L. Improved fluorescent probes for the measurement of rapid changes in membrane potential. *Biophys. J.* **1982**, *39*, 301−308.
(42) Grinvald, A.; Fine, A.; Farber, I. C.; Hildesheim, R. Fluorescence monitoring of electrical responses from small neurons and their processes. *Biophys. J.* **1983**, *42*, 195−198.
(43) Amoroso, S.; Agon, V. V.; Starke-Peterkovic, T.; McLeod, M. D.; Apell, H.-J.; Sebban, P.; Clarke, R. J. Photochemical behaviour and Na^+,K^+-ATPase sensitivity of voltage-sensitive styrylpyridinium fluorescent membrane probes. *Photochem. Photobiol.* **2006**, *82*, 495−502.
(44) Clarke, R. J.; Kane, D. J. Optical detection of membrane dipole potential: avoidance of fluidity and dye-induced effects. *Biochim. Biophys. Acta, Biomembr.* **1997**, *1323*, 223−239.
(45) Grinvald, A.; Frostig, R. D.; Lieke, E.; Hildesheim, R. Optical imaging of neuronal activity. *Physiol. Rev.* **1988**, *68*, 1285−1366.

https://doi.org/10.1021/acs.langmuir.4c04779
Langmuir XXXX, XXX, XXX−XXX

(46) Clarke, R. J.; Zouni, A.; Holzwarth, J. F. Voltage sensitivity of the fluorescent probe RH421 in a model membrane system. *Biophys. J.* **1995**, *68*, 1406−1415.
(47) Visser, N. V.; van Hoek, A.; Visser, A. J. W. G.; Frank, J.; Apell, H.-J.; Clarke, R. J. Time-resolved fluorescence investigations of the interaction of the voltage-sensitive probe RH421 with lipid membranes and proteins. *Biochemistry* **1995**, *34*, 11777−11784.
(48) Kane, D. J.; Fendler, K.; Grell, E.; Bamberg, E.; Taniguchi, K.; Froehlich, J. P.; Clarke, R. J. Stopped-flow investigations of conformational changes of pig kidney. *Biochemistry* **1997**, *36*, 13406−13420.
(49) Batzri, S.; Korn, E. D. Single bilayer liposomes prepared without sonication. *Biochim. Biophys. Acta, Biomembr.* **1973**, *298*, 1015−1019.
(50) Vitha, M. F.; Clarke, R. J. Comparison of excitation and emission ratiometric fluorescence methods for quantifying the membrane dipole potential. *Biochim. Biophys. Acta, Biomembr.* **2007**, *1768*, 107−114.
(51) Pintschovius, J.; Fendler, K. Investigation on solid supported membranes: Rapid solution exchange with a new technique. *Biophys. J.* **1999**, *76*, 814−826.
(52) Garcia-Celma, J. J.; Hatahet, L.; Kunz, W.; Fendler, K. Specific anion and cation binding to lipid membranes investigated on a solid supported membrane. *Langmuir* **2007**, *23*, 10074−10080.
(53) Tadini-Buoninsegni, F.; Bartolommei, G. Electrophysiological measurements on solid supported membranes. *Methods Mol. Biol.* **2016**, *1377*, 293−303.
(54) Tadini-Buoninsegni, F.; Fendler, K. Recording of pump and transporter activity using solid-supported membranes (SSM-based electrophysiology). In *Pumps, Channels, and Transporters. Methods of Functional Analysis*; Clarke, R. J.; Khalid, M. A. A., Eds.; Wiley: Hoboken, U.S.A., 2015; pp 147−177.
(55) Bazzone, A.; Barthmes, M.; Fendler, K. SSM-based electrophysiology for transporter research. *Methods Enzymol.* **2017**, *594*, 31−83.
(56) Bazzone, A.; Barthmes, M. Functional characterization of SLC transporters using solid supported membranes. *Methods Mol. Biol.* **2020**, *2168*, 73−103.
(57) Clarke, R. J.; Lüpfert, C. Influence of anions and cations on the dipole potential of phosphatidylcholine vesicles: A basis for the Hofmeister effect. *Biophys. J.* **1999**, *76*, 2614−2624.
(58) Clarke, R. J.; Apell, H.-J. A stopped-flow kinetic study of the interaction of potential-sensitive oxonol dyes with lipid vesicles. *Biophys. Chem.* **1989**, *34*, 225−237.
(59) Clarke, R. J. Binding and diffusion kinetics of the interaction of a hydrophobic potential-sensitive dye with lipid vesicles. *Biophys. Chem.* **1991**, *39*, 91−106.
(60) Frank, J.; Zouni, A.; van Hoek, A.; Visser, A. J. W. G.; Clarke, R. J. Interaction of the fluorescent probe RH421 with ribulose-1,5-bisphosphate carboxylase/oxygenase and with Na^+,K^+-ATPase membrane fragments. *Biochim. Biophys. Acta, Biomembr.* **1996**, *1280*, 51−64.
(61) Clarke, R. J. Dipole-potential-mediated effects on ion pump kinetics. *Biophys. J.* **2015**, *109*, 1513−1520.
(62) Pearlstein, R. A.; Dickson, C. J.; Hornak, V. Contributions of the membrane dipole potential to the function of voltage-gated cation channels and modulation by small molecule potentiators. *Biochim. Biophys. Acta, Biomembr.* **2017**, *1859*, 177−194.
(63) Sarkar, P.; Chattopadhyay, A. Membrane dipole potential: An emerging approach to explore membrane organization and function. *J. Phys. Chem. B* **2022**, *126*, 4415−4430.

https://doi.org/10.1021/acs.langmuir.4c04779
Langmuir XXXX, XXX, XXX−XXX